

Consistent Acetonitrile Molecular Models for both Standard and Computationally Efficient Molecular Dynamics Studies

H. Ariel Alvarez ^{1,2}, Carlos Llerena Suster ³ and Andrés N. McCarthy ^{1,2*}

¹Instituto de Física de Líquidos y Sistemas Biológicos (IFLYSIB) - 49 N° 789, B1900BTE - La Plata, Argentina (UNLP - CONICET).

² Departamento de Ciencias Biológicas, Facultad de Ciencias Exactas, Universidad Nacional de La Plata.

³ Laboratorio de Investigación en Proteínas Vegetales (LIPROVE), Fac. Cs. Exactas – UNLP.
E-mail: amccarthy {at} iflysib.unlp.edu.ar

ABSTRACT— *Acetonitrile is widely utilized in scientific research, presenting an ideal solvent media for a large number of organic reactions. Its use at the industrial scale ranges from the production of molecules of pharmaceutical interest to photographic films. Additionally, certain enzyme based catalytic processes show great functionality in Acetonitrile media. Furthermore, numerous enzymes continue to act as efficient biocatalyzers in acetonitrile solution, showing in some cases significant changes in their original specificity and selectivity. Consequently, the study of the behavior of such proteins in this solvent by means of potent computational methods such as Molecular Dynamics results of great interest. Many molecular models for Acetonitrile have been developed for use in Molecular Dynamic studies. Nevertheless, all acetonitrile models developed up to date are only capable of performing reasonably when used with integration time-steps no greater than 2 femtoseconds (fs). We present two molecular models for acetonitrile which perform both efficiently and reliably with integration time steps of up to 4 fs. Furthermore, the optimization procedure used has enabled to achieve this performance improvement at no cost as regards the agreement between the experimental macroscopic data for Acetonitrile and the corresponding properties evaluated for the models here presented.*

Keywords--- Acetonitrile; Three-site Models; Molecular Dynamics; Integration Time-step Scalability.

1. INTRODUCTION

Acetonitrile is one of the most widely utilized solvents in scientific research. Being miscible with water, of intermediate polarity, low viscosity and scarce reactivity, it is capable of dissolving a wide variety of ionic and non-polar compounds, and is a very useful mobile phase in HPLC studies.

It is an ideal solvent for a large number of organic reactions. It is also used as a solvent in the manufacturing of many products of the most diverse nature, ranging from molecules of pharmaceutical interest to photographic films at the industrial scale.

Acetonitrile is an appropriate solvent for processes that use enzymes as catalysts. This is both due to its ability to easily solubilize reaction reagents and products, as well as its capacity to provide a highly polar reaction media, allowing nevertheless total absence of water, which in general causes high inhibition of most synthesis reactions [1,2,3].

Notably, numerous enzymes continue to act as efficient biocatalyzers in acetonitrile solution [4,5,6,7,8]. Additionally, organic solvent media is known to produce alterations in the secondary and tertiary structures of many enzymes, producing notable modifications both in their selectivity and specificity [1].

Thus, the study of the behavior of such proteins in this solvent, particularly using simulation methods such as Molecular Dynamics, becomes both interesting and necessary, constituting a promising approach to achieve a better understanding of such systems.

Many molecular models for Acetonitrile have been developed for use in Molecular Dynamic studies. Their degree of detail ranges from models with six explicit sites [9,10] (one per atom), to the more simplified three site models (which treat the methyl hydrogens and their carbon as a unique site) [11,12,13,14,15,16].

Whilst three site models greatly reduce computational cost, their performance has proven comparable to the more detailed, and computationally expensive, six site models. Nevertheless, all acetonitrile models developed up to date are only capable of performing reasonably when used with integration time-steps no greater than 2 femtoseconds (fs).

Given that presently a number of highly validated protein forcefields may be used with integration time-steps of 4 fs, the development of a model for Acetonitrile which performs correctly at these longer integration time-steps becomes highly desirable. Such is the objective of the present work.

The 2 fs integration time-step limit arises from the natural oscillation of the angle between the Methyl-Carbon bond and the Carbon-Oxygen bond. Such limitation can not be resolved by introducing a larger angle bending harmonic potential, given that the oscillation frequency is proportional to the square root of such a constant. Thus, these models become inherently restricted to be used only under standard integration time step conditions.

In this work we present a molecular model for acetonitrile which has the capacity of performing correctly under integration time steps of up to 4 fs. Nevertheless, this feature comes at no cost as regards its degree of correspondence with ACN experimental macroscopic magnitudes, whilst it enables to double time performance of simulation runs.

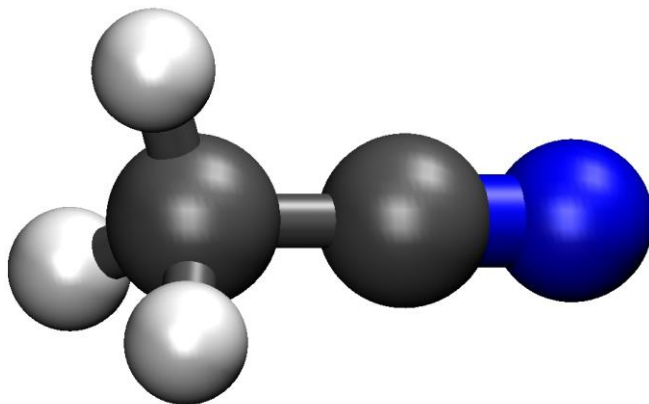


Figure 1 - Schematic structure of Acetonitrile

2. MATERIALS AND METHODS

2.1 LAM - The proposed model

The model we propose for acetonitrile molecule (*LAM* model) may be regarded as a quasi-three-site model. Namely, three sites were assigned for electric charge distribution as well as for Lennard-Jones (L-J) interaction centers, whilst the mass distribution was treated through a two site approach, as shown in Figure 2.

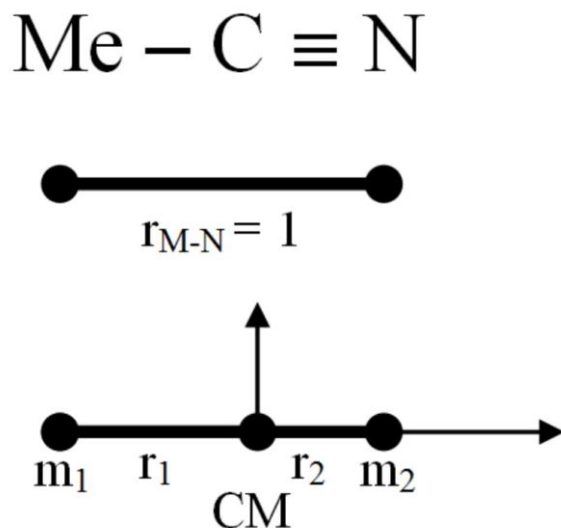


Figure 2 - Schematic mass distribution for Acetonitrile

The six atomic masses present in the Acetonitrile molecule were reduced to a two site mass distribution, treated as virtual sites, under the following constraint conditions:

- Same position for the centre of mass (COM).
- Same Moment of inertia with respect to the axis that crosses the COM.
- Distance between m_1 and m_2 equal to Methyl-Nitrogen Distance.
- Total Mass of 41.0527 amu.

From the above considerations we obtain the following values for both masses and positions:

$$m_1 = 9.49031 \text{ a.m.u.}$$

$$m_2 = 31.56239 \text{ a.m.u.}$$

$$r_1 = 0.7650$$

$$r_2 = 0.2350$$

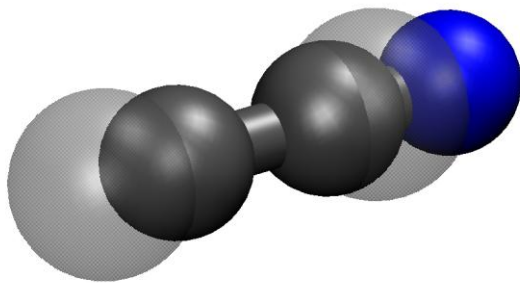


Figure 3 - A representation of the relative position of masses (transparent view) and charges/L-J interaction centers (solid view).

Figure 3 shows a representation of the relative position for the resulting two site mass distribution (transparent view) relative to the three site distribution for both charges and L-J interaction centers (solid view).

2.2 Simulation Details

We carried out the Molecular Dynamics (MD) simulations using the GROMACS 4 Package. For the calculation of electrostatic forces we applied the Reaction Field method. Lennard–Jones interactions were calculated within a cut-off radius of 1.4 nm.

We analyzed systems comprised of 512 acetonitrile molecules, at a fixed temperature of 298K and pressure of 1bar, using the V-rescale thermostat [17] and the Berendsen barostat [18] respectively.

All NPT MD simulations consisted of 1.5 ns long molecular dynamic runs, using both 2 fs and 4 fs integration time-steps.

In order to assess the performance of every model studied under such conditions, their ability to reproduce the following macroscopic observables was evaluated: Density (ρ), Isothermal Compressibility (κ_T), Isobaric Thermal Expansion Coefficient (α), Enthalpy of Vaporization (H_v), Molecular Reorientational Correlation Times (τ_1, τ_2), Self-Diffusion Coefficient (D), Dielectric Permittivity (ϵ) and Debye Relaxation Time (τ_D). Structural and conformational properties of all the developed models were studied by calculating every site-site Radial Distribution Function $g(r)$. Additional simulation runs were performed at 273K and 323K, in order to evaluate the Isobaric Heat Capacity (C_p). Likewise, Shear Viscosity (η) was evaluated by performing additional short (100ps) runs, on systems comprised of 512 and 1024 Acetonitrile molecules.

In order to determine the integration accuracy performance of *LAM* models, simulations in the microcanonical (NVE) ensemble were performed, with neither temperature nor pressure coupling. Reaction-Field-Zero scheme was used for long range electrostatic interactions, which optimizes energy conservation with reaction field. Simulations were performed in double precision for a total simulation time of 20 ps. Production data was collected from the last 10 ps.

Two independent criteria were applied to assess the 2 and 4 fs integration accuracy performance of the proposed models.

The first quantifier is given by the ratio between the fluctuation in total energy $\langle \Delta E^2 \rangle^{1/2}$ and the total energy average $\langle E \rangle$; i.e. $\langle \Delta E^2 \rangle^{1/2} / \langle E \rangle$ [19].

Complementarily, the kinetic to total energy fluctuation ratio, given by $\langle \Delta E^2 \rangle^{1/2} / \langle \Delta KE^2 \rangle^{1/2}$, where the denominator is the square root of the fluctuations in the kinetic energy of the system, was also evaluated [20]. These two criteria scale differently with the size of the simulated system, as the total energy is proportional to N (the total number of atoms in the system), whilst the kinetic energy fluctuation increases with $N^{1/2}$ [20].

As regards different integration algorithms, it has been established that, for small time steps, higher order integration methods provide increased accuracy [20,21,22]. However, such higher order methods are more sensitive to the truncation of long range forces, particularly when using integration time-steps greater than 1 fs [20], thus rendering here the leap-frog algorithm as an adequate choice for the integration of MD equations of motion.

2.3 LAM Model Optimization Procedure

The values of the L-J coefficients were used as variables in the model optimization procedure. Charge distribution values were fixed to those proposed by *Guardia et al.* [13].

The optimization procedure was performed following two concurrent, yet distinct, approaches. The first approach consisted in solely adjusting the L-J collision diameter for the Methyl group, whilst the second approach allowed for simultaneous optimization adjustments, applied over the L-J collision diameters of both the Methyl group and the central Carbon atom, using equal values for the correction ratio. The models obtained from each approach were named *LAM-A* and *LAM-B* respectively. The model used as input for the optimization procedure (*LAM-0*) has the same fixed charge distribution values proposed by *Guardia et al.* [13], with all L-J collision diameters unchanged.

The performance of every model studied with modified *LAM* parameters was assessed as previously described.

The differences between calculated and experimental values, for every macroscopic observable studied, were simultaneously compared. Subsequently, the obtained differences were plotted against the variation percentage applied to each L-J collision diameter parameter. Finally, a minimization of the polynomial function that better adjusted the data was performed.

The optimal values for the L-J parameter variation percentages that result from the procedure described above are 3% for the *LAM-A* model and 2% for the *LAM-B* model.

The actual optimal values obtained for the L-J collision diameter parameters are shown in Table 1.

Table 1 - Lennard-Jones parameters for the optimized *LAM* models studied compared to those of *Gee & van Gunsteren* and *Guardia et al.*

Magnitude	Gee & van Gunsteren [14]	Guardia et al. [13]	LAM-A	LAM-B
Lennard-Jones Coefficients				
C ₆ [10 ⁻³ kJmol ⁻¹ nm ⁶]	C _{6Me} = 9.491654 C _{12Me} = 1.68584	C _{6Me} = 9.057 C _{12Me} = 2.621	C _{6Me} = 7.544 C _{12Me} = 1.8185	C _{6Me} = 8.0242 C _{12Me} = 2.0567
C ₁₂ [10 ⁻⁵ kJmol ⁻¹ nm ¹²]	C _{6C} = 1.765738 C _{12C} = 0.222702	C _{6C} = 5.145 C _{12C} = 1.217	C _{6C} = 5.145 C _{12C} = 1.217	C _{6C} = 4.5577 C _{12C} = 0.955
	C _{6N} = 1.475272 C _{12N} = 0.155459	C _{6N} = 2.696 C _{12N} = 0.2894	C _{6N} = 2.696 C _{12N} = 0.2894	C _{6N} = 2.696 C _{12N} = 0.2894

2.4 Calculation of the Selected Macroscopic Observables

Enthalpy of Vaporization:

The Enthalpy of Vaporization was calculated using the following expression:

$$\Delta H_{vap} = -U_{liq}(T) + p\Delta V + \Delta H_{real-ideal} \quad (1)$$

where U_{liq} is the Potential Energy per mol of the system, $p\Delta V$ is the expansion work at 298K and 1atm, which is taken as equal to that of the ideal gas under the same thermodynamical conditions ($p\Delta V = 2.479 \text{ kJ/mol}$). The enthalpy difference between the real and ideal gas was estimated as: $\Delta H_{real-ideal} = 0.5 \pm -0.2 \text{ kJ/mol}$ [23].

Dielectric Permittivity:

The dielectric permittivity of the system was obtained from a Clausius-Mosotti type equation [24], considering the dipolar moment of the single molecule as μ (3.96 D), and the relative dielectric permittivity of the Reaction Field as ϵ_{RF} (35.86) [25].

Debye Relaxation Time:

We consider the system to behave as a single Debye dielectric, i.e., one with a frequency dependent dielectric permittivity $\epsilon(\omega)$ given by,

$$\epsilon(\omega) = \epsilon_{\infty} + \frac{\epsilon_s - \epsilon_{\infty}}{1 + i\omega\tau_D} \quad (2)$$

where ϵ_s is the static dielectric permittivity, ϵ_{∞} is the high-frequency limit permittivity and τ_D is the Debye relaxation time. Once $\epsilon(\omega)$ has been obtained, τ_D may be determined from the low-frequency behaviour.

$$\tau_D = \lim_{\omega \rightarrow 0} \frac{\epsilon_s - \epsilon(\omega)}{i\omega(\epsilon(\omega) - \epsilon_{\infty})} \quad (3)$$

Self Diffusion Coefficient:

The self diffusion coefficient D was evaluated using the Einstein relation [26],

$$\lim_{t \rightarrow \infty} \langle \|r_i(t) - r_i(0)\|^2 \rangle = 6Dt \quad (4)$$

where $r_i(t)$ is the position vector of each atom at time t , and the averaging over all atoms is indicated by $\langle \rangle$.

Isobaric Heat Capacity:

The isobaric heat capacity was evaluated from the expression used by *Gee and van Gunsteren* [14]:

$$C_p = \frac{E_{tot2} - E_{tot1}}{T_2 - T_1} + \frac{\partial E_{int}}{\partial T} + \frac{\partial E_{ext}}{\partial T} \quad (5)$$

The total energy of the system in the first term was considered performing two simulation runs, at temperatures 25 K above and below the temperature of the reference system, 298 K (i.e. 323K and 273K).

The second term introduces a correction to the rigid treatment of bonds and bond angles $\left(\frac{\partial E_{int}}{\partial T} = 0.035 \frac{J}{K} \cdot mol \right)$.

The third term is a second order correction that takes into account the quantum-mechanical features of the liquid, and has been neglected.

Shear viscosity:

The method proposed by Palmer [27] was used for the evaluation of shear viscosity, performing two short (100ps) runs with 512 and 1024 molecules respectively at 298K. In this method, a quadratic relationship between the viscosity and the wave vector is assumed:

$$\eta(k) = \eta_{\infty} + ak^2 \quad (6)$$

The value of the shear viscosity η_{∞} is obtained from the $k \rightarrow \infty$ limit for $\eta(k)$.

Isothermal compressibility:

The Isothermal compressibility is calculated based on the fluctuation formula [22]

$$\kappa_T = -\frac{1}{V} \left(\frac{\partial V}{\partial p} \right)_T = \frac{\langle \delta V^2 \rangle}{k_B T \langle V \rangle} \quad (7)$$

where V , p and T represent the volume, pressure and temperature of the system, δ indicates fluctuations, and the angular brackets denote ensemble expectation values in NPT conditions.

Isobaric Thermal Expansion Coefficient:

We calculated the Isobaric Thermal Expansion Coefficient from fluctuations on volume and Enthalpy H [22].

$$\alpha = \frac{1}{V} \left(\frac{\partial V}{\partial T} \right)_p = \frac{\langle \delta V \delta H \rangle}{k_B T^2 \langle V \rangle} \quad (8)$$

Molecular Reorientational Correlation Times:

We computed the reorientational correlation times τ_l ($l=1, 2$). We performed these calculations fitting the exponential decay function, e^{-t/τ_l} , to the reorientational correlation function, $C_l(t)$, defined as:

$$C_l(t) = \langle P_l(\bar{e}(t) \cdot \bar{e}(0)) \rangle \quad (9)$$

where $\bar{e}(t)$ denotes the unit vector pointing along the molecule axis at time t , P_l is the l th-order Legendre polynomial ($l = 1, 2$) and $\langle \rangle$ denotes time averaging. Reported values were obtained from an exponential fit to the correlation function in the range 5–10 ps.

3. RESULTS AND DISCUSSION

3.1 Site-site Radial Distribution Functions

All site-site radial distribution functions $g_{ij}(r)$ (with $i, j = \text{Me, C, N}$) computed from the MD simulations are presented in Figure 4. The six different correlation functions are represented separately. Each graph shows four different curves, which correspond to the results calculated for both models in each integration step condition (black: *LAM-B* 2 fs; red: *LAM-B* 4 fs; green: *LAM-A* 2 fs; blue: *LAM-A* 4 fs).

From the evaluation of Figure 4 we may readily observe that all four models show very similar correlational behavior, both regarding model differences and time-step integration conditions. The slight differences that appear in the first peak of the C-C, N-N and Me-N correlation functions may be readily explained as a consequence of the Lennard-Jones parameter modifications applied in the model optimization procedure.

On the whole, these results indicate that differences between models and integration step conditions result almost negligible as regards their short range liquid structural behavior.

3.2 Results under 2 fs integration time-step simulation conditions

Table 2 shows the results obtained for the proposed *LAM* acetonitrile models, for every macroscopic observable studied, under 2 fs integration time-step simulation conditions. The values of the macroscopic observables, as published in literature [13,14], are also presented for two of the previously developed acetonitrile models. Additionally, in order to allow further performance comparison between models, the 2 mass distribution correction was applied to the acetonitrile models *Guardia et al.* [13] and *Gee & van Gunsteren* [14]. The resulting models were denominated *LAM-0* and *LAM-1* respectively.

3.2.1 Density:

The density comparison shows the best concordance for the *LAM-A* model, followed by the *LAM-B* model, with the *Gee & van Gunsteren* model in the third place. Nevertheless, all three models present a reasonable concordance with experimental data.

3.2.2 Enthalpy of Vaporization:

In the case of the Enthalpy of Vaporization, the best concordance is shown by the *LAM-0* model, closely followed by the *Gee & van Gunsteren* model, with the *LAM-B* model in the third place. Notably, all three models present very similar absolute value differences with experiment, although the *LAM-0* model underestimates the Enthalpy of Vaporization, whilst both the *Gee & van Gunsteren* model and the *LAM-B* model overestimate this observable.

3.2.3 Isobaric Heat Capacity:

When analyzing the Isobaric Heat Capacity, the best concordance is shown by the *Guardia et al.* model, followed by the *LAM-0* model, again presenting a close third place for the *LAM-B* model. Remarkably, both three mass models overestimate the Isobaric Heat Capacity, whilst all two mass models produce an underestimation of this observable. Additionally, it may be noted that all models studied present very similar absolute value differences with experiment.

3.2.4 Shear viscosity:

As regards Shear Viscosity, the best concordance is shown by the *LAM-0* model, followed by the *LAM-B* model, with the *LAM-1* model in the third place. Here, the two mass models show a better performance than their three mass counterparts. Additionally, it is notable that, in the case of Shear Viscosity, the different models studied show the greatest relative differences in their ability to reproduce the experimental value of Acetonitrile.

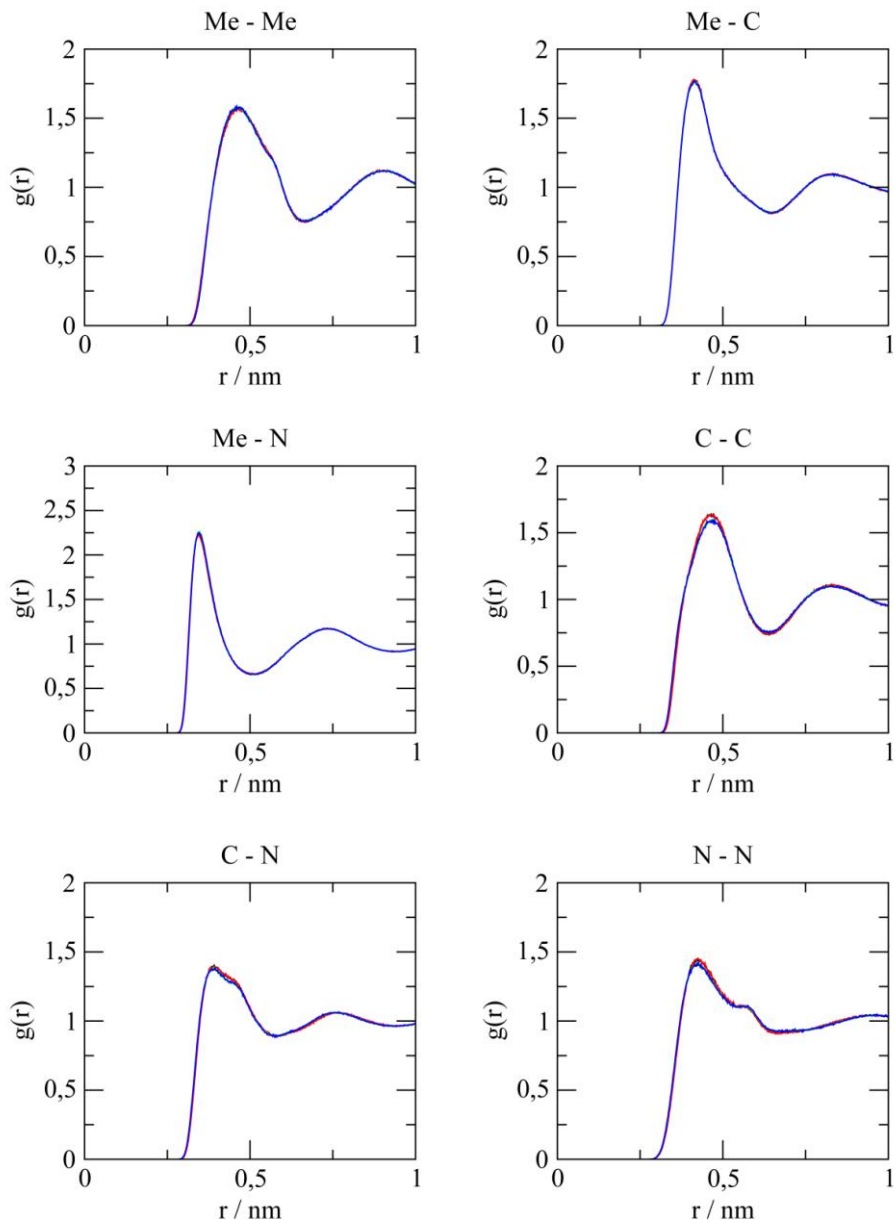


Figure 4 - All site-site radial distribution functions $g_{ij}(r)$ (with $i, j = \text{Me}, \text{C}, \text{N}$) computed from the MD simulations are presented, for *LAM-A* and *LAM-B* models, under 2 and 4 fs integration time-step conditions (black: *LAM-B* 2 fs; red: *LAM-B* 4 fs; green: *LAM-A* 2 fs; blue: *LAM-A* 4 fs)

3.2.5 Self Diffusion Coefficient:

In the case of the Self Diffusion Coefficient, the best concordance is shown by the *Gee & van Gunsteren* model, followed by the *LAM-O* model, with the *LAM-A* model in third place. As in the case of the Enthalpy of Vaporization, all models present differences greater than five percent with the experimental value. Nevertheless, in the case of Self Diffusion Coefficient, the models studied show important relative differences to approximate the actual experimental behavior. Additionally, it may be noted that all models overestimate this observable.

3.2.6 Dielectric Permittivity:

The comparison of the Dielectric Permittivity shows a clear advantage for the *Gee & van Gunsteren* model, far followed by its own counterpart, the *LAM-I* model, with a close third place for the *LAM-B* model. Additionally, in the case of Dielectric Permittivity, the different models studied show very high relative differences in their ability to reproduce the experimental value

of Acetonitrile, only second to the relative difference variability shown for Shear Viscosity.

3.2.7 Debye Relaxation Time:

In the case of the Debye Relaxation Time, the best concordance is shown by the *LAM-1* model, closely followed by the *Guardia et al.* model, with the *Gee & van Gunsteren* model in the third place. Notably, all three models overestimate this observable.

3.2.8 Isothermal compressibility:

When analyzing the Isothermal compressibility, the best concordance is shown by the *LAM-0* model, followed by the *LAM-A* model with a close third place for the *LAM-B* model. Once more, all three models overestimate this observable.

3.2.9 Isobaric Thermal Expansion Coefficient:

As regards the Isobaric Thermal Expansion Coefficient, the *LAM-0* model shows the best behavior, followed by the *LAM-A* model, again presenting a close third place for the *LAM-B* model. Here again all three models overestimate this observable.

3.2.10 Molecular Reorientational Correlation Times:

τ_1 : The comparison of τ_1 shows a clear advantage for the *LAM-B* model, followed by the *LAM-A* model, and a close third place for the *LAM-0* model. Although with very low error percentage values, here again all three models overestimate this observable.

τ_2 : A clear advantage of the *LAM-0* model is observed, followed by the *Gee & van Gunsteren* model, with a close third place for the *LAM-A* model. In this case the error percentage values are notably greater, showing overestimation by the first two models and underestimation by the last.

Table 2 - Macroscopical magnitudes corresponding to the proposed *LAM* acetonitrile models are shown, together with available reference experimental data. The corresponding values for *Gee & van Gunsteren* and *Guardia et al.* models are shown, as found in literature. Additionally, presently obtained results for models *LAM-0* and *LAM-1* (which result from applying the 2 mass distribution correction to acetonitrile models *Guardia et al.* [13] and *Gee & van Gunsteren* [14] respectively) are presented.

Magnitude	Gee & van Gunsteren		LAM-1		Guardia et al.		LAM-0		LAM-A		LAM-B		Experimental
	Value	% Difference	Value	% Difference	Value	% Difference	Value	% Difference	Value	% Difference	Value	% Difference	
Density [kg m ⁻³]	764.00	1.67	881.69	-13.47	634.00	18.40	743.70	4.29	777.35	-0.05	774.43	0.33	777.00 [28]
ΔH_{vap} [kJ mol ⁻¹]	32.70	2.39	39.03	-16.50	27.60	17.61	34.27	-2.30	34.91	-4.21	34.56	-3.16	33.50 [29]
C _p [10 ⁻² kJ mol ⁻¹ K ⁻¹]	7.84	14.41	10.75	-17.31	7.98	12.88	10.42	-13.73	10.47	-14.28	10.46	-14.18	9.16 [30]
Viscosity [cP]	0.29	14.71	0.36	-7.06	0.64	-88.24	0.34	-0.59	0.37	-9.84	0.33	2.13	0.34 [31]
Self Diff. Coeff. D [10 ⁹ m ² s ⁻¹]	3.73	7.67	2.49	38.31	6.55	-62.13	3.63	10.15	3.41	15.61	3.11	22.93	4.04 [32]
Dielectric Permittivity ϵ [adimensional]	35.30	1.51	40.81	-13.86	22.70	36.66	26.02	27.40	30.67	14.41	31.71	11.52	35.84 [25]
Isothermal compressibility κ_T [10 ¹⁰ Pa ⁻¹]	-	-	6.12	25.09	6.40	21.66	7.35	10.04	6.75	17.38	6.44	21.18	8.17 [33]
Isobaric Thermal Expansion Coefficient α [10 ⁻⁴ K ⁻¹]	-	-	12.09	11.82	-	-	13.67	0.29	13.23	3.50	12.17	11.23	13.71 [34]
Molecular Reorientational Correlation Times τ_1 [ps]	1.93	41.16	4.38	-33.54	3.55	-8.23	2.88	12.20	3.21	1.98	3.26	0.48	3.28 [35]
Molecular Reorientational Correlation Times τ_2 [ps]	0.80	21.57	1.31	-28.43	1.45	-42.16	0.88	13.73	1.30	-26.97	1.33	-30.70	1.02 [Error! Bookmark not defined.]
Debye Relaxation Time τ_D [ps]	2.20	35.29	2.88	15.29	2.60	23.53	1.90	44.12	1.82	46.47	2.12	37.65	3.40 [25]
Sum of % Difference Modules *		140.38		183.78		309.84		128.49		133.81		123.08	
Comparative Global Model Performance		4th		5th		6th		2nd		3rd		1st	

3.2.11 Total Sum of the Model-Experiment Difference Percentage Modules:

In order to quantify the general performance of the models under study, the total sum of every model-experiment difference percentage module was calculated. Thus, an overall relative comparison between the different models may be established.

According to the previously proposed overall performance quantifier, the best general performance, using a 2 fs integration time-step, is shown by the *LAM-B* model, closely followed by the *LAM-O* model, with an even closer third place for the *LAM-A* model.

Thus, the *LAM-B* model comes as the best choice for performing molecular dynamic studies with standard integration time-steps, particularly when seeking reasonable overall performance. Nevertheless, when the ability to reproduce either Self Diffusion or Dielectric Permittivity is of relevance, the *Gee & van Gunsteren* model performs more accurately.

3.3 Results under 4 fs integration time-step simulation conditions

Table 3 presents the results obtained for the proposed *LAM* acetonitrile models, for every macroscopic observable studied, using an integration time-step of 4 fs. Additionally, in order to allow for further evaluation of the *LAM* models, Table 3 reproduces the macroscopic observables for models *LAM-O* and *LAM-I*, as obtained by the present study. Due to the inability of 3-mass models to perform under 4 fs integration time-step simulation conditions, no data is available in Table 3 for the *Gee & van Gunsteren* and *Guardia et al.* models.

3.3.1 Density:

The density comparison shows the best concordance for the *LAM-A* model, followed by the *LAM-B* model, with the *LAM-O* model in the third place. All three models present a reasonable concordance with experimental data.

3.3.2 Enthalpy of Vaporization:

As in the previous conditions, in the case of the Enthalpy of Vaporization the best concordance is shown by the *LAM-O* model, closely followed nevertheless by the *LAM-B* model, with a very close third place for the *LAM-A* model. All three models present very similar absolute value differences with experiment. Additionally, they also all slightly underestimate the experimental value of the Enthalpy of Vaporization for Acetonitrile.

3.3.3 Isobaric Heat Capacity:

When analyzing the Isobaric Heat Capacity, the best concordance is shown by the *LAM-O* model, closely followed by the *LAM-A* model, again presenting a very close third place for the *LAM-B* model. All models produce an underestimation of this observable. It may be noted that all models studied present very similar absolute value differences with experiment.

3.3.4 Shear viscosity:

As regards Shear Viscosity, the best concordance is here shown by the *LAM-A* model, closely followed by the *LAM-B* model, with the *LAM-O* model relatively far back in the third place. Again, the different models studied show a great relative difference in their ability to reproduce the experimental value of Acetonitrile.

3.3.5 Self Diffusion Coefficient:

In the case of the Self Diffusion Coefficient, the best concordance is shown by the *LAM-O* model, closely followed by the *LAM-B* model, with an also close third place occupied by the *LAM-A* model. All models present differences greater than ten percent with the experimental value. Contrarily to the behavior observed under shorter integration time-step conditions, in the case of Self Diffusion Coefficient, all models studied show low relative differences as regards their ability to approximate experimental behavior. Again, it may be noted that all models overestimate this observable.

3.3.6 Dielectric Permittivity:

The comparison of the Dielectric Permittivity shows a clear advantage for the *LAM-I* model, far followed by the *LAM-A* model, with a clear third place for the *LAM-O* model. As under the shorter integration time-step conditions, the different models studied show very high relative differences in their ability to reproduce the experimental value of Acetonitrile.

3.3.7 Debye Relaxation Time:

In the case of the Debye Relaxation Time, the best concordance is shown by the *LAM-1* model, closely followed by the *LAM-B*, with the *LAM-A* model in the third place. As with 2 fs integration time-steps, all three models overestimate this observable.

3.3.8 Isothermal compressibility:

When analyzing the Isothermal compressibility, the best concordance is shown by the *LAM-0* model, followed by the *LAM-A* model and a close third place for the *LAM-B* model. As before, all three models overestimate this observable.

Table 3 - Macroscopical magnitudes corresponding to the proposed *LAM* acetonitrile models are shown, together with available reference experimental data. Additionally, the results obtained for models *LAM-0* and *LAM-1* (which result from applying the 2 mass distribution correction to acetonitrile models *Guardia et al.* [13] and *Gee & van Gunsteren* [14] respectively) are presented.

Magnitude	Gee & van Gunsteren		LAM-1		Guardia et al.		LAM-0		LAM-A		LAM-B		Experimental
	Value	% Difference	Value	% Difference	Value	% Difference	Value	% Difference	Value	% Difference	Value	% Difference	
Density [kg m ⁻³]	-	-	881.800	-13.5	-	-	746.800	3.9	776.87	0.0	773.9	0.4	777.00 [Error! Bookmark not defined.]
ΔH_{vap} [kJ mol ⁻¹]	-	-	39.025	-16.5	-	-	34.259	-2.3	34.89	-4.1	34.54	-3.1	33.50 [Error! Bookmark not defined.]
C _p [10 ² kJ mol ⁻¹ K ⁻¹]	-	-	10.760	-17.5	-	-	10.414	-13.7	10.46	-14.2	10.48	-14.4	9.16 [Error! Bookmark not defined.]
Viscosity [cP]	-	-	0.447	-31.5	-	-	0.364	-7.1	0.3397	0.1	0.344	-1.2	0.34 [Error! Bookmark not defined.]
Self Diff. Coeff. D [10 ⁹ m ² s ⁻¹]	-	-	2.585	36.0	-	-	3.490	13.6	3.38	16.3	3.46	14.4	4.04 [Error! Bookmark not defined.]
Dielectric Permittivity ϵ [adimensional]	-	-	33.991	5.2	-	-	26.459	26.2	29.1	18.8	26.35	26.5	35.84 [25]
Isothermal compressibility κ_T [10 ¹⁰ Pa ⁻¹]	-	-	6.320	22.6	-	-	7.140	12.6	6.83	16.4	6.65	18.6	8.17 [Error! Bookmark not defined.]
Isobaric Thermal Expansion Coefficient α [10 ⁻⁴ K ⁻¹]	-	-	12.720	7.2	-	-	13.180	3.9	13.51	1.5	12.25	10.6	13.71 [Error! Bookmark not defined.]
Molecular Reorientational Correlation Times τ_1 [ps]	-	-	4.410	-34.5	-	-	2.880	12.2	3.218	1.9	3.2557	0.7	3.28 [Error! Bookmark not defined.]
Molecular Reorientational Correlation Times τ_2 [ps]	-	-	1.330	-30.4	-	-	0.880	13.7	1.3142	-28.8	1.2996	-27.4	1.02 [Error! Bookmark not defined.]
Debye Relaxation Time τ_D [ps]	-	-	2.570	24.4	-	-	2.100	38.2	2.18	35.9	2.24	34.1	3.40 [25]
Sum of % Difference Modules				239.22				147.32		138.06		151.45	
Comparative Global Model Performance				4th				2nd		1st		3rd	

3.3.9 Isobaric Thermal Expansion Coefficient:

As regards the Isobaric Thermal Expansion Coefficient, the *LAM-A* model shows the closest accordance, followed by the *LAM-O* model, presenting here a close third place for the *LAM-I* model. Again, all three models overestimate this observable.

3.3.10 Molecular Reorientational Correlation Times:

τ_1 : The comparison of τ_1 consistently shows a clear advantage for the *LAM-B* model, followed by the *LAM-A* model, with the *LAM-O* model in third place. Although with very low error percentage values, all three models overestimate this observable.

τ_2 : The *LAM-O* model shows here clear advantage, followed by the *LAM-B* model, and a close third place for the *LAM-A* model. In this case the error percentage values are notably greater, showing overestimation by the first model and underestimation by the last two.

3.3.11 Total Sum of the Model-Experiment Difference Percentage Modules:

The total sum of the modules of each model-experiment difference percentage was calculated, thus establishing an overall relative comparison between the different models. From the data presented in Table 3 we can conclude that, when using a 4 fs integration time-step, the best general performance is shown by the *LAM-A* model, closely followed by the *LAM-O* model, with the *LAM-B* model in the third place.

Consequently, under these higher integration time-step conditions, the models here proposed would constitute, *a priori*, a reasonable choice.

If a balanced overall performance is needed, the *LAM-B* model would here constitute a reasonable choice. Nevertheless, if the ability to reproduce either Isobaric Heat Capacity or Density were of greater relevance, the *LAM-A* model would here come as a preferred option. On the other hand, the eventual use of the *LAM-I* model should only be regarded for simulation studies, performed under 4 fs integration time-step conditions, where the importance of the Dielectric Permittivity precludes almost every other macroscopic parameter.

3.4. Assessment of the integration accuracy

The proposed models integration accuracy performance using 2 fs and 4 fs integration time-steps was assessed through the evaluation of two different quantifiers; i.e. Total Energy Fluctuation over Average Ratio and Total over Kinetic Energy Fluctuation Ratio.

Given that the Total Energy is proportional to N (number of atoms in the system) whilst the Kinetic Energy fluctuation increases with $N^{1/2}$, these quantifiers scale differently with the simulated system size [20]. Consequently, both parameters were studied in order to better evaluate the integration accuracy performance of the models hereby presented.

3.4.1 Total Energy Fluctuation over Average Ratio:

This quantifier is defined as the ratio between the fluctuation in total energy $\langle \Delta E^2 \rangle^{1/2}$ and the total energy average $\langle E \rangle$; i.e. $\langle \Delta E^2 \rangle^{1/2} / \langle E \rangle$ [19].

For liquid state simulations, $\langle \Delta E^2 \rangle^{1/2} / \langle E \rangle$ should be less than 0.01% [19].

3.4.2 Total over Kinetic Energy Fluctuation Ratio:

This quantifier, calculated as the ratio e kinetic to is given by $\langle \Delta E^2 \rangle^{1/2} / \langle \Delta KE^2 \rangle^{1/2}$, where the numerator is the total energy fluctuation and the denominator is the fluctuation in the kinetic energy, both as calculated for the total system [20].

Most authors suggest that acceptable values for this quantity should be in the range of or below 1-10% [20,21,22].

The data obtained for both models is presented in Table 4. The results show (for both LAM models presented, both quantifiers studied, and both integration time-step conditions) values roughly tenfold within (smaller than) the accepted limits, as established by reference literature [19,20,21,22].

Additionally, as regards their high integration accuracy performance, no significant differences are observed between both *LAM* models.

These results show that both acetonitrile *LAM* models perform efficiently in the microcanonical ensamble (NVE), with clear energy conservation capacity, both under 2 fs and 4 fs integration time-step conditions.

Table 4 - Data obtained for both integration accuracy performance quantifiers studied; i.e. Total Energy Fluctuation over Average Ratio $\langle \Delta E^2 \rangle^{1/2} / \langle E \rangle$ and Total over Kinetic Energy Fluctuation Ratio $\langle \Delta E^2 \rangle^{1/2} / \langle \Delta KE^2 \rangle^{1/2}$. Both Acetonitrile *LAM* models were evaluated using 2 fs and 4 fs integration time-steps.

Model	timestep [fs]	Kinetic Energy [kJ.mol ⁻¹]		Total Energy [kJ.mol ⁻¹]		$\langle \Delta E^2 \rangle^{1/2} / \langle \Delta KE^2 \rangle^{1/2}$	$\langle \Delta E^2 \rangle^{1/2} / \langle E \rangle$
		Kinetic Energy Average $\langle KE \rangle$	Kinetic Energy Fluctuation $\langle \Delta KE^2 \rangle^{1/2}$	Total Energy Average $\langle E \rangle$	Total Energy Fluctuation $\langle \Delta E^2 \rangle^{1/2}$		
LAMA	2fs	6356,30	69,96	-26718,80	0,12	0,00171938	0,00000450
	4fs	6371,28	69,34	-26605,50	0,31	0,00445377	0,00001161
LAMB	2fs	6365,54	70,88	-26326,00	0,14	0,00190553	0,00000513
	4fs	6362,30	68,90	-26282,60	0,34	0,00489138	0,00001282

3.5 Results and Discussion Summary

The present Molecular Dynamic simulation studies performed under standard integration time-step conditions, for both *LAM* models proposed, reveal their ability to reproduce numerous macroscopic properties of acetonitrile, rendering (at the very least) a performance comparable to that of the top 3-mass models previously developed. Thus, as discussed before, the *LAM* models could be a correct choice when simulation studies aimed to achieve a balanced overall system performance. Furthermore, when high integration time-step conditions are needed, both *LAM* models could be regarded as a reasonable choice.

4. CONCLUSIONS

The *LAM* Acetonitrile models presented perform correctly, reliably and comparably, using both 2 fs and 4 fs integration time steps.

Under standard (2 fs) integration time-step simulation conditions, these models show an equivalent overall performance to that of the other reference 3-mass Acetonitrile models studied available in literature. Nevertheless, it should be noted that the three site model proposed by *Gee & van Gunsteren* presents a notable higher ability to reproduce the Dielectric Permittivity experimental value of Acetonitrile than every other model studied. Thus, when performing a study where such a property were of main interest, the *Gee & van Gunsteren* model should clearly be used. Likewise, when performing a study where either Density, Shear Viscosity, Isothermal Compressibility, Isobaric Thermal Expansion Coefficient or Molecular Reorientational Correlation Times, result of main interest, either *LAM-A* or *LAM-B* models could result reasonable choices. Additionally, it should be noted that under standard (2 fs) integration time-step simulation conditions, the *LAM-B* model presents the best balance in overall performance.

As regards high (4 fs) integration time-step conditions, both *LAM* models perform efficiently and reliably, making this a unique feature to the proposed models.

Summarizing, when using standard integration time-steps, the *LAM* models may be regarded as of comparable performance to that of the *Gee & van Gunsteren* model, and could be used complementarily, according to the objectives pursued in a particular MD study involving the use of a model for acetonitrile.

As regards situations in which the computational efficiency becomes a fundamental issue (i.e. 4 fs integration time-step conditions), the use of either of the *LAM* models become reasonable choices.

5. AKNOWLEDGEMENTS

This work was partially supported by the Consejo Nacional de Investigaciones Científicas y Técnicas of Argentina (CONICET), the University of La Plata, the Comisión Científica de la Provincia de Buenos Aires (CICPBA) and the Agencia Nacional de Promoción Científica y Tecnológica de Argentina (ANPCyT).

6. REFERENCES

- ¹ Bordusa, F., *Proteases in Organic Synthesis*. Chemical Reviews, 2002. **102**(12): p. 4817-4868.
- ² Morcelle, S.R., et al., *Comparative behaviour of proteinases from the latex of Carica papaya and Funastrum clausum as catalysts for the synthesis of Z-Ala-Phe-OMe*. Journal of Molecular Catalysis B: Enzymatic, 2006. **41**(3-4): p. 117-124.
- ³ Morcelle, S.R., et al., *Screening of plant peptidases for the synthesis of arginine-based surfactants*. Journal of Molecular Catalysis B: Enzymatic, 2009. **57**(1-4): p. 177-182.
- ⁴ Simon, L.M., Kotormán, M., Szabo, A., Nemcsók, J., Laczkó I. (2007). *The effects of organic solvent/water mixtures on the structure and catalytic activity of porcine pepsin*. Proc Bioch, **42** : 909-912.
- ⁵ Simon, L.M., Lázló, K., Vértesi, A., Bagi, K., Szajáni, B. (1998). *Stability of hydrolytic enzymes in water-organic solvent systems*. J. Mol Catal B: Enzymatic, **4** : 41-45.
- ⁶ Szabó, A., Kotormán, M., Laczkó, I., Simon, L.M. (2006). *Spectroscopic studies of stability of papain in aqueous organic solvents*. J. Mol. Catal. B: Enzymatic, **41**: 43-48.
- ⁷ Kijima, T., Yamamoto, S., Kise, H. (1996). *Study on tryptophan fluorescence and catalytic activity of α -chymotrypsin in aqueous-organic media*. Enzyme and Microbial Technology. **18** : 2-6.
- ⁸ C. R. Llerena-Suster, C. José, S. E. Collins, L. E. Briand, S. R. Morcelle. *Investigation of the structure and proteolytic activity of papain in aqueous miscible organic media*. Process biochemistry **47** (2012), 47-56.
- ⁹ Böhm, H.J., et al., *Molecular motion in a model of liquid acetonitrile*. Molecular Physics: An International Journal at the Interface Between Chemistry and Physics, 1984. **51**(3): p. 761 - 777.
- ¹⁰ Nikitin, A.M. and A.P. Lyubartsev, *New six-site acetonitrile model for simulations of liquid acetonitrile and its aqueous mixtures*. Journal of Computational Chemistry, 2007. **28**(12): p. 2020-2026.
- ¹¹ Edwards, D.M.F., P.A. Madden, and I.R. McDonald, *A computer simulation study of the dielectric properties of a model of methyl cyanide -- I. The rigid dipole case*. Molecular Physics: An International Journal at the Interface Between Chemistry and Physics, 1984. **51**(5): p. 1141 - 1161.
- ¹² Jorgensen, W.L. and J.M. Briggs, *Monte Carlo simulations of liquid acetonitrile with a three-site model*. Molecular Physics: An International Journal at the Interface Between Chemistry and Physics, 1988. **63**(4): p. 547 - 558.
- ¹³ Guàrdia, E., et al., *Comparison of Different Three-site Interaction Potentials for Liquid Acetonitrile*. Molecular Simulation, 2001. **26**(4): p. 287 - 306.
- ¹⁴ Gee, P.J. and W.F. van Gunsteren, *Acetonitrile revisited: a molecular dynamics study of the liquid phase*. Molecular Physics: An International Journal at the Interface Between Chemistry and Physics, 2006. **104**(3): p. 477 - 483.
- ¹⁵ Wick, C.D., et al., *Transferable Potentials for Phase Equilibria. 7. Primary, Secondary, and Tertiary Amines, Nitroalkanes and Nitrobenzene, Nitriles, Amides, Pyridine, and Pyrimidine*. The Journal of Physical Chemistry B, 2005. **109**(40): p. 18974-18982.
- ¹⁶ Hirata, Y., *Molecular Dynamics Simulation Study of the Rotational and Translational Motions of Liquid Acetonitrile*. The Journal of Physical Chemistry A, 2002. **106**(10): p. 2187-2191.
- ¹⁷ C.C. Huang, A. Chatterji, G. Sutmann, G. Gompper, R.G. Winkler, *Cell-level canonical sampling by velocity scaling for multiparticle collision dynamics simulations*. J. Comput. Phys. **229**(1): 168-177, 2010.
- ¹⁸ Berendsen, H. J. C., Postma, J. P. M., DiNola, A., Haak, J. R. *Molecular dynamics with coupling to an external bath*. J. Chem. Phys. **81**:3684–3690, 1984.
- ¹⁹ M. P. Allen and D. J. Tildesley, Oxford Science Publications, Clarendon Press, **Oxford** (1987).

- ²⁰ W F. van Gunsteren and H. J. C. Berendsen, Mol. Phys., **34**, 1311 (1977).
- ²¹ J. C. Berendsen and W F. van Gunsteren, in Molecular Liquids: Dynamics and Interactions; J. Barnes et al. Eds., NATO ASI Series, **C135**, 475; Reidel, Dordrecht (1984).
- ²² M. Levitt, J. Mol. Biol., **168**, 595 (1983).
- ²³ An, X.-W. and M. Måansson, *Enthalpies of combustion and formation of acetonitrile*. The Journal of Chemical Thermodynamics, 1983. **15**(3): p. 287-293.
- ²⁴ Spoel, D.v.d., P.J.v. Maaren, and H.J.C. Berendsen, *A systematic study of water models for molecular simulation: Derivation of water models optimized for use with a reaction field*. Vol. **108**. 1998: AIP. 10220-10230.
- ²⁵ Barthel, J., M. Kleebauer, and R. Buchner, *Dielectric relaxation of electrolyte solutions in acetonitrile*. Journal of Solution Chemistry, 1995. **24**(1): p. 1-17.
- ²⁶ Allen, M.P. and D.J. Tildesley, *Computer Simulation of Liquids*. 1989: Oxford University Press, USA.
- ²⁷ Palmer, B.J., *Transverse-current autocorrelation-function calculations of the shear viscosity for molecular liquids*. Physical Review E, 1994. **49**(1): p. 359.
- ²⁸ Gallant, R. W., *Physical properties of hydrocarbons. XXXVI. Nitriles*, Hydrocarbon Process., 1969. **48**, 135.
- ²⁹ An, X.-W. and M. Måansson, *Enthalpies of combustion and formation of acetonitrile*. The Journal of Chemical Thermodynamics, 1983. **15**(3): p. 287-293.
- ³⁰ Wagman, D.D., et al., *The NBS tables of chemical thermodynamic properties : selected values for inorganic and C1 and C2 organic substances in SI units*. 1982. **11**(1).
- ³¹ Cunningham, G.P., G.A. Vidulich, and R.L. Kay, *Several properties of acetonitrile-water, acetonitrile-methanol, and ethylene carbonate-water systems*. Journal of Chemical & Engineering Data, 1967. **12**(3): p. 336-337.
- ³² Kovacs, H., et al., *M multinuclear relaxation and NMR self-diffusion study of the molecular dynamics in acetonitrile-chloroform liquid mixtures*. The Journal of Physical Chemistry, 1989. **93**(2): p. 962-969.
- ³³ Narayanaswamy, G., G. Dharmaraju, and G.K. Raman, *Excess volumes and isentropic compressibilities of acetonitrile +n-propanol, +i-propanol, +n-butanol, +i-butanol, and +cyclohexanol at 303.15 K*. The Journal of Chemical Thermodynamics, 1981. **13**(4): p. 327-331.
- ³⁴ Grant-Taylor, D.F. and D.D. Macdonald, *Thermal pressure and energy-volume coefficients for the acetonitrile + water system*. Canadian Journal of Chemistry, 1976. **54**(17): p. 2813-2819.
- ³⁵ Yuan, P. and M. Schwartz, *Molecular reorientation in acetonitrile. A comparison of diffusion coefficients from Raman bandshapes and nuclear magnetic resonance relaxation times*. Journal of the Chemical Society, Faraday Transactions, 1990. **86**(4): p. 593-596.